

Nernst–Planck modeling of multicomponent ion transport in a Nafion membrane at high current density

S. Moshtarikhah¹ · N. A. W. Oppers¹ · M. T. de Groot² · J. T. F. Keurentjes¹ · J. C. Schouten¹ · J. van der Schaaf¹

Received: 13 June 2016 / Accepted: 18 October 2016 / Published online: 1 November 2016
© The Author(s) 2016. This article is published with open access at Springerlink.com

Abstract A mathematical model of multicomponent ion transport through a cation-exchange membrane is developed based on the Nernst–Planck equation. A correlation for the non-linear potential gradient is derived from current density relation with fluxes. The boundary conditions are determined with the Donnan equilibrium at the membrane–solution interface, taking into account the convective flow. Effective diffusivities are used in the model based on the correlation of tortuosity and ionic diffusivities in free water. The model predicts the effect of an increase in current density on the ion concentrations inside the membrane. The model is fitted to the previously published

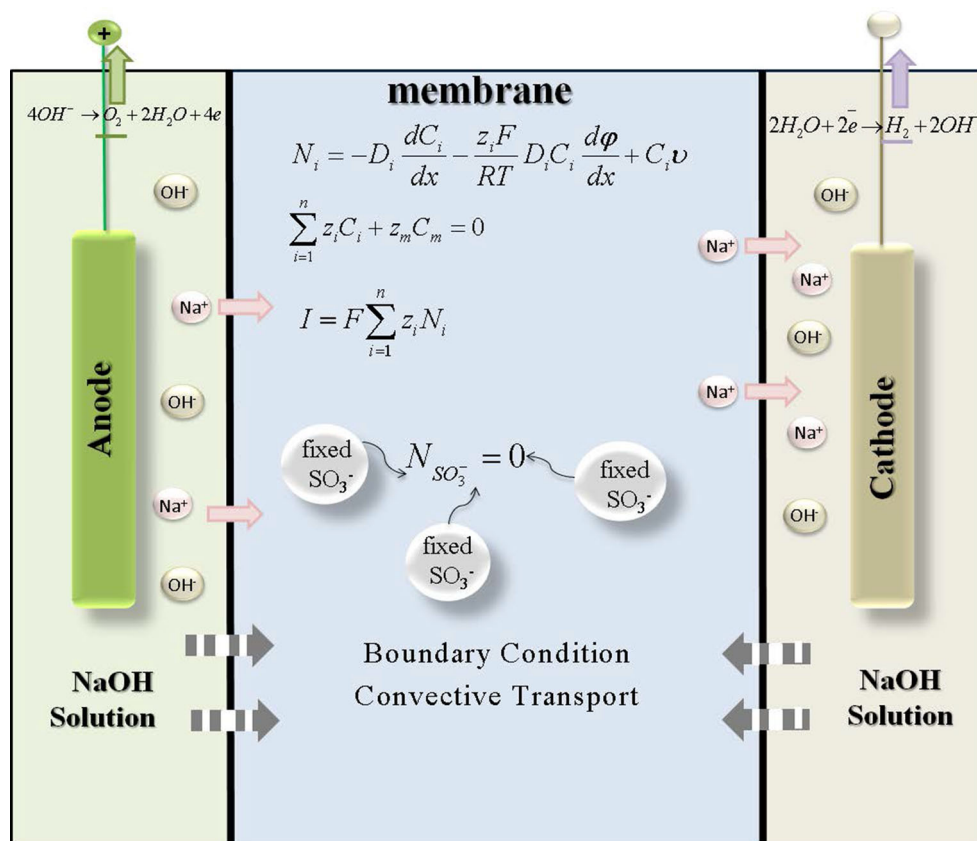
experimental data. The effect of current density on the observed increase in voltage drop and the decrease in permselectivity has been analyzed using the available qualitative membrane swelling theories. The observed non-linear behavior of the membrane voltage drop versus current density can be explained by an increase in membrane pore diameter and an increase in the number of active pores. We show how the membrane pore diameter increases and dead-end pores open up when the current density is increased.

✉ J. van der Schaaf
j.vanderschaaf@tue.nl

¹ Eindhoven University of Technology, P.O. Box 513,
5600 MB Eindhoven, The Netherlands

² Akzo Nobel industrial Chemicals B.V.,
P.O. Box 247, 3800 AE Amersfoort, The Netherlands

Graphical Abstract



Keywords Multicomponent ion transport · Nernst–Planck · Membrane resistivity · Membrane selectivity · High current density

List of symbols

Latin symbols

a	Activity coefficient
A	Membrane cross-sectional area (m^2)
C	Concentration ($mol\ m^{-3}$)
d_h	Hydrodynamic permeability ($kg.s.m^{-3}$)
d_p	Pore diameter (m)
D	Diffusion coefficient ($m^2\ s^{-1}$)
D_{ij}	Effective diffusion coefficient ($m^2\ s^{-1}$)
f	Fraction in cluster (–)
F	Faraday constant ($C\ mol^{-1}$)
h_f	Hydration factor (–)
I	Current density ($A\ m^{-2}$)
J	Flux ($mol\ m^{-2}\ s^{-1}$)
K	Donnan equilibrium constant (–)
$K_{anolyte}$	Mass transfer coefficient in anolyte ($m\ s^{-1}$)
N	Number of pore channels (–)
P	Pressure (Pa)
r	Radius (m)
R	Gas constant ($J\ mol^{-1}\ K^{-1}$)

t	Time (s)
t_i	Ion transport number (–)
T	Temperature (K)
W	Weight percentage (wt%)
x	Length (m)
x'	Dimensionless length (–)
V	Volume (m^3)
\bar{V}	Partial molar volume ($m^3\ mol^{-1}$)
z_i	Valence (–)
z	Dimensionless length (–)

Greek symbols

δ	Membrane thickness (m)
ϕ	Electrical potential (V)
Δ	Difference (–)
∇	Gradient (–)
κ	Conductivity ($ohm^{-1}\ m^{-1}$)
ρ	Density ($g\ cm^{-3}$)
μ	Chemical potential ($J\ mol^{-1}$)
η	Dynamic viscosity (Pa s)
v	Convective volume flux ($m^3\ m^{-2}\ s^{-1}$)
ε	Porosity (–)
τ	Tortuosity (–)
λ	Actual pore length (m)

Superscript and subscript

act	Active
A	Anode
Am	Anolyte-membrane
c	Centigrade
Cm	Catholyte-membrane
Don	Donnan
e	Electrolyte
i	Species
int	Interface
L	Left
m	Membrane
p	Pore
R	Right
s	Solution phase
tot	Total
w	Water

1 Introduction

Ion-exchange membranes have several industrial applications, including fuel cells, the Chlor–Alkali process, and water electrolysis. In order to explain the mass transfer in the membrane at high current densities, a suitable mathematical model is required. There are different approaches to describe the transport of ions inside the membrane. Rohman and Aziz have reviewed mathematical models of ion transport in electrodialysis. They have proposed three types of phenomenological equations in their irreversible thermodynamic approach: (1) the Maxwell–Stefan (MS) equation which takes the interaction between each pair of components into account; (2) the Kedem–Katchalsky (KK) equation that considers the membrane as a geometric transition region between two homogenous compartments; and (3) the Nernst–Planck (NP) equation which describes diffusion and electro-migration in the ionic transport without taking into account the interaction between ions. The latter is widely used because of its simplicity [1]. Psaltis et al. have compared the Nernst–Planck and Maxwell–Stefan approaches to transport predictions of ternary electrolytes. They have concluded that using binary diffusivities (neglecting interaction between different solute species) and the full Maxwell–Stefan model does not affect the final steady-state concentrations profiles in the electrolyte solution of a multicomponent system. This shows that using the effective diffusivities in the Nernst–Planck equation should give reasonable accuracy in the results [2]. Additionally, Graham et al. have shown that the Nernst–Planck equation is valid in modeling diffusion of ions in ion-exchange resins of high concentrations (3–4 M) if taking into account the effective diffusivities [3].

The morphological structure of an ion-exchange membrane is also important in modeling the transport process in the pore volume of the membrane. This is because any change in the morphology, i.e., the number and size of liquid pores, can alter the effective diffusivities inside the pores and as a result the transport process. There have been several studies on the morphological structure of ion-exchange membranes, particularly the Nafion membrane, i.e., core–shell model proposed by Fujimura et al. [4], a sandwich-like model proposed by Haubold et al. [5], and a rod-like model proposed by Rubatat et al. [5]. The cluster-network model presented by Mauritz et al. [6] is one of the earliest models widely used for understanding the properties of Nafion membranes. This model is based on small-angle X-ray scattering (SAXS) measurements and estimates the cluster network of Nafion to consist clusters with a diameter of ~ 4 nm with 1-nm channels connecting the pore clusters. Also, among the early models, Yeager et al. proposed a three-phase model without any strict geometry of the clusters with an interphase between the hydrophobic and hydrophilic regions [6]. Schmidt et al. simulated parallel water channel models for the structure of the Nafion membrane with water channel diameters of 1.8 and 3.5 nm with an average of 2.4 nm at 20 vol% water [7]. Gebel et al. have studied the structural evolution of perfluoro-sulfonated ionomer membranes from dry to a highly swollen state with small-angle X-ray scattering (SAXS) measurement [8]. They characterized the structural evolution of Nafion 115 and 117 of 1100 EW. They concluded that as the membrane gets hydrated and swells, the cluster sizes increase. As a result of opening up of the pores, the pore clusters connect. At even higher hydration level, the authors observed that the swelling process for water content larger than 50 % causes an inversion of the structure from a reverse micellar structure to a connected network of polymer rod-like particles [8]. Based on their assumption for water swollen state, the cluster radii is 2 nm and it increases to 2.09, 2.18, and 2.35 nm for the case of *N*-methylformamide, ethanol, and formamide, respectively [8].

The transport of ions in the membrane with the Nernst–Planck approach has been studied by other authors as well. Verbrugge et al. [9] have developed ion and solvent transport within a sulfuric acid/perfluorosulfonic acid membrane. Bouzek et al. [10, 11] also modeled the ion transport inside the membrane with and without considering the convection in the diffusion layer. They predict the ion transport in the membrane up to 2.5 kA m^{-2} .

The purpose of this work is to develop a Nernst–Planck model that can describe the transport of ions in the membrane at high current densities. It is of great interest to understand the membrane performance in terms of voltage drop and permselectivity at high current densities, because

the membrane has the biggest contribution to the cell voltage. Thus, it is vital to include the membrane performance in the assessment of the electrochemical cell performance and the process economics. In this study, the transport of species inside the pore volume of the membrane is described taking into account the effective diffusivities. Also, the morphological structure of the membrane in this study is based on the model from Schmidt et al. and Gebel because they give an indication of the size of channel diameters in dry and hydrated states. One difference to the approach in this study and the work of Verbrugge et al. [9] is that they use an empirical correlation for the partition coefficient at the solution–membrane interface. Here, a general Donnan equilibrium phenomenon is used to describe the boundary condition. In the work of Bouzek et al. [10, 11], the model is already assumed to be at steady-state and therefore requires accurate initial guesses to avoid convergence errors. In this study, the model is time-dependent and not sensitive to initialization. Also, Bouzek et al. use self-diffusion coefficients estimated by others, whereas here the free solution diffusivities are used to estimate diffusivities in the membrane. This is done by evaluating the channel size and porosity of the membrane. Additionally, the focus of this work is on the membrane performance at high current densities.

The Nernst–Planck model is fitted to experiments which are elaborated elsewhere [12]. The potential drop over the membrane and the membrane selectivity are determined from the ionic fluxes in the membrane for current densities up to 20 kA m⁻² and in a 15 wt% sodium hydroxide solution.

2 Model approach

The Nernst–Planck equation for modeling the transport of ions in an ion-exchange membrane for an ideal solution can be written as Eq. (1) [13, 14]:

$$J_i = -D_i \nabla C_i - z_i D_i C_i \frac{F}{RT} \nabla \varphi + C_i v. \quad (1)$$

It consists of three transport terms: diffusion, electro-potential, and convection. The convection term is affected by the osmotic pressure and electro-osmotic effects, and it can be defined as Eq. (2) with the Schlögl equation [9, 15]. Electroneutrality is assumed everywhere in the membrane and at the interface of the membrane and solution (Eq. 3).

$$v = d_h (z_m C_m F \nabla \varphi - \nabla P), \quad (2)$$

$$\sum_i C_i z_i = 0. \quad (3)$$

Schlögl has defined the hydrodynamic permeability of the membrane based on Hagen–Poiseuille presented in Eq. (4) [16]:

$$d_h = \frac{d_p^2 \epsilon_m}{32 \eta}. \quad (4)$$

The Schlögl equation seems to be able to describe the convective velocity as a constant value in the membrane. Additionally, the mass continuity correlation (Eq. 6) is required to complete the system of transport equations. This means that the convective velocity needs to be defined at every position in the membrane. This is because the density changes with the variation of concentration inside the membrane. The convective velocity is calculated based in Eq. (2) at the left side of the membrane with an initial guess of the membrane voltage drop. Then, using the sodium hydroxide density correlation (Eq. 5) [17], the convective velocity is determined at every position inside the membrane. The relation between the current density and the flux of charged species is shown in Eq. (7). Equation (8) is derived by combining Eqs. (1) and (7) as an expression for the potential gradient. The voltage drop from Eq. (8) is then iterated using an initial guess until the solution is converged.

Equation (9) describes the water flux. The concentration of water inside the membrane is calculated based on the concentration of sodium and hydroxide ions at every position using the density correlation (Eq. (5)). It has been shown by several authors [12, 18–21] that water is not only transported in the hydrated shell of the positive ions, but also due to convection and the electromotive force.

$$\rho \times 10^{-3} = 1.006 + 0.0011 W_{\text{NaOH}} - 0.172 \times 10^{-4} W_{\text{NaOH}}^2 - 0.358 \times 10^{-3} T_c - 0.214 \times 10^{-5} T_c^2, \quad (5)$$

$$-\nabla(\rho v) = 0, \quad (6)$$

$$I = F \sum_{i=1}^n z_i J_i, \quad (7)$$

$$\nabla \varphi = \frac{\frac{I}{F} + \sum_{i=1}^n z_i D_i \nabla C_i - v \sum_{i=1}^n z_i C_i}{-\frac{F}{RT} \sum_{i=1}^n z_i^2 D_i C_i}, \quad (8)$$

$$\rho v = \sum_{\substack{i=1 \\ n \neq \text{water}}}^n M_i N_i + M_{\text{water}} N_{\text{water}}. \quad (9)$$

In literature, the electrical conductivity of a membrane has been defined based on Ohm's law, $I = \kappa \frac{d\varphi}{dx}$, using the Nernst–Planck flux equation, and also by neglecting the concentration gradient and convection [13, 14, 17]. This is debatable to be valid since our experimental results [12] show that the membrane conductivity depends not only on concentration and temperature but also on the current density. Additionally, we show here in Appendix A that the potential gradient is not constant, and its non-linear behavior is required to have equal fluxes at the left and right sides of the membrane at the steady-state condition.

Equations (1) to (8) make the system of transport equations inside the membrane complete without taking into account the water dissociation effect. Water dissociation, proton, and hydroxyl ion production due to self-ionization of water is more important in anion-exchange membranes than in cation-exchange membranes [22–32]. Tanaka has studied the mechanism of concentration polarization and water dissociation in the boundary layer of ion-exchange membranes. He has shown that the water dissociation in the strong acid cation-exchange membrane is more suppressed than in the strong base anion-exchange membrane because the forward reaction rate constant in the cation-exchange membrane is lower. In fact, due to stronger repulsive forces between the fixed ionic groups of the cation-exchange membrane and the co-ions, the water dissociation reaction is suppressed [32]. Also, this study is at a high concentration of the electrolyte solution which is not known to cause water dissociation.

2.1 Boundary conditions [13, 33, 34]

For the boundary condition, the flux of species at the steady-state should be equal at the membrane and solution interface which is shown in Eq. (10) for anode interface. This is similar for the cathode interface. The mass transfer at the membrane surface is assumed very high because of the very high mixing of the electrolyte at the membrane surface which is elaborated in our earlier paper [12]. Thus, the boundary layer thickness is calculated from the measured mass transfer in a rotor–stator spinning disc reactor which is proved to have a very high mass transfer coefficient [35]. The concentration jump of ionic species at the solution and the membrane interface for both anolyte and catholyte sides are depicted in Fig. 1.

$$\frac{D_i^s}{\delta_{diff}} (C_i^{A,s} - C_i^{A,int}) + \nu C_i^{A,int} \varepsilon = \left(-D_i \frac{dC_i^{Am,int}}{dx'} - z_i D_i C_i^{Am,int} \frac{F}{RT} \frac{d\varphi}{dx'} + \nu C_i^{Am,int} \delta \right) \frac{1}{\delta} \varepsilon. \tag{10}$$

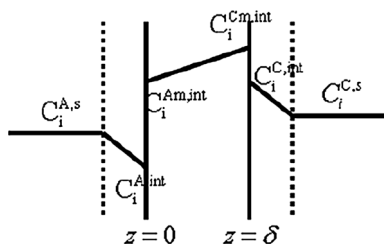


Fig. 1 Schematic drawing of the concentration of ionic species in the bulk solution, at the solution, and at the membrane interface for both anolyte and catholyte sides

The concentrations at the interface are defined based on the Donnan equilibrium phenomenon which is an electrochemical equilibrium between the membrane and solution phases (Eq. 11). At steady-state in equilibrium, the electrochemical potential of all ions in the membrane and the solution are equal [13]:

$$\mu_i^m + z_i F \varphi^m = \mu_i^s + z_i F \varphi^s. \tag{11}$$

The Donnan potential can be expressed with Eq. (12):

$$\varphi^m - \varphi^s = \frac{1}{z_i F} \left[RT \ln \frac{a_i^s}{a_i^m} + \bar{V}_i (P^s - P^m) \right] = \varphi_{Don}. \tag{12}$$

Here, the assumption of Higa et al. [34] that the surface of the membrane is always in the state of Donnan equilibrium with the same partition coefficient for all of the ions is used. This way the Donnan equilibrium gives a general correlation for all ions between the membrane and the external solution. This is shown in Eq. (13) in which the osmotic pressure is neglected:

$$\frac{C_i^m}{C_i^s} = e^{\frac{-Fz_i \Delta\varphi_{Don}}{RT}} = K^{z_i}. \tag{13}$$

We have used the electroneutrality condition in the solution to derive a correlation (Eq. 14) that relates the solution interface concentration and the membrane interface concentration (See Appendix 3).

$$C_{i,pos}^{A,int} = C_{i,pos}^{m,0} \sqrt{\frac{\sum_i^{N_{ions}} C_{i,neg}^{m,0}}{\sum_i^{N_{ions}} C_{i,pos}^{m,0}}}, \tag{14}$$

$$C_{i,neg}^{A,int} = C_{i,neg}^{m,0} \sqrt{\frac{\sum_i^{N_{ions}} C_{i,pos}^{m,0}}{\sum_i^{N_{ions}} C_{i,neg}^{m,0}}}.$$

It is also possible to define the membrane interface concentration based on the solution interface concentration using the electroneutrality condition in the membrane. However, it might require solving a quartic, quintic, etc. equations depending on the valence and the number of ions. This makes it more complicated to be solved.

2.2 Solver

The pdepe solver of MATLAB is used. It iterates the system of equations over time and uses one-dimensional space to obtain the solution at the steady state. The complete set of dimensionless equations is presented in detail in Appendix 2. The grid points are set in a logarithmic scale near the boundaries due to a larger gradient of concentration and linear in the center part.

2.3 Model assumptions

Constant pressure and temperature are assumed. The pressure contribution in the transport equations and Donnan equilibrium approach is neglected especially because the same concentration of sodium hydroxide as anolyte and catholyte is being used. Solutions are assumed to be ideal. Properties of the Nafion single-layer membrane, N-1110 [36], are used.

2.4 Constitutive equations

The initial water concentration inside the membrane is calculated based on the water uptake for perfluorinated membrane of 1100 EW as a function of sodium hydroxide concentration. The water uptake is presented in weight percentage of dry polymer in Eq. (15) [17].

$$W_w = -0.0052 \times (0.001C_{\text{NaOH}})^3 + 0.165 \times (0.001C_{\text{NaOH}})^2 - 2.708 \times (0.001C_{\text{NaOH}}) + 36.68. \quad (15)$$

In a polymeric matrix, the path length of diffusion is not a straight line. Thus, diffusion coefficients of ionic species in free water are used and converted into effective diffusivities. This is shown in Eq. (16) where the diffusivities in the polymer matrix and in the free water are related via tortuosity [37].

$$D_{ij} = D^s_{ij}/\tau. \quad (16)$$

The dependency of tortuosity to the polymer porosity has been shown in many models in the literature [38–41]. Here, the model predicted by Marshal which was used by Wesselingh is used to define the tortuosity as presented in Eq. (17) [37].

$$\tau = \varepsilon^{-1.5}. \quad (17)$$

Equation (18) defines the porosity of the membrane as the volume of pores with ion clusters divided by the total volume.

$$\varepsilon = \frac{V_e f_e}{V_{\text{tot}}} = \frac{\frac{W_e}{\rho_e}}{\frac{1}{\rho_m} + \frac{W_e}{\rho_e}} f_e. \quad (18)$$

W_e and ρ_e which are the weight fraction and the density of the adsorbed electrolyte are estimated based on the water uptake of the membrane (W_o in Eq. 15) and the density of the water. f_e is the fraction of electrolyte in the pores with ion cluster; it is estimated based on the work of Yeo et al. [42] to be 0.76. This gives an estimation of the membrane porosity as a constant parameter in the model. Also, the membrane is assumed to have stationary fixed charges and to consist of homogenous cylindrical channels. The concentration of the stationary fixed charges in the membrane

is calculated from Eq. (19). It takes into account the density and weight fraction of the adsorbed electrolyte, equivalent weight (EW), which is defined as the weight of polymer in gram per mole of sulfonic acid groups, fraction of ionic groups, and electrolyte in the ion cluster [17, 42].

$$C_m = \frac{1000 \times \rho_e}{EW \times W_e} \left(\frac{f_m}{f_e} \right). \quad (19)$$

It has been discussed in literature that a Nafion membrane swells when hydrated [4–6, 8, 43]. After the model simulation with constant porosity and channel diameter, the ion transport through the membrane at high current densities is assumed to follow a similar trend as when the hydration level increases in the membrane. Apparently, increasing the current density results in opening up of the pore clusters and opening of the dead-end pores [6]. According to Takahashi et al. [44], the channel size should be dependent on the relationship between the inner stress due to the pressure inside the channel and the elasticity of the polymer matrix. Thus, due to higher mass flux under high current density, the inner stress increases and results in opening up of the pore channels [44]. The change in the pore size and opening of the dead-end pores are depicted in Fig. 2.

Here, the assumption of the membrane swelling based on the work of Tiss et al. is used when performing the sensitivity analysis of the model. They assumed that the channels are oriented in the same direction in the membrane and are perpendicular to the membrane–liquid interface. The membrane porosity, which is the occupied volume fraction of the membrane by liquid, is assumed to have N number of cylindrical channels (N^{tot}) per cross-

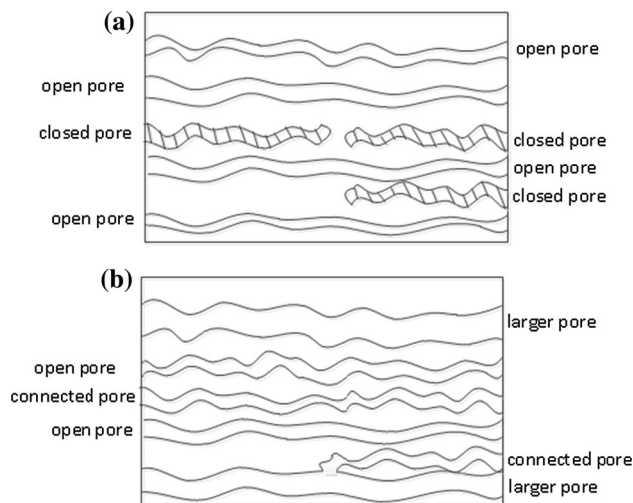


Fig. 2 Simplified sketch of the membrane cross-sectional area consisting of homogenous cylindrical channels with open (active) pores and closed (inactive) pores of a **a** non-swollen membrane and **b** swollen membrane at high current densities

sectional area. By taking into account the tortuosity effect, the total porosity can be calculated with Eq. (20):

$$\varepsilon^{\text{tot}} = N^{\text{tot}} \pi r_p^2 \tau. \tag{20}$$

Combining Eqs. (17) and (20), the total and active porosities of the membrane are defined as a function of the total number of pores (N^{tot}) and the pore radius (r_p) in Eqs. (21) and (22).

$$\varepsilon^{\text{tot}} = (N^{\text{tot}} \pi r_p^2)^{\frac{2}{5}}, \tag{21}$$

$$\varepsilon^{\text{act}} = (N^{\text{act}} \pi r_p^2)^{\frac{2}{5}}. \tag{22}$$

The transport number presented in Eq. (23) is the fraction of current carried by a certain ion. It is an indication of the membrane permselectivity.

$$t_i = \frac{J_i \times F}{I}. \tag{23}$$

2.5 Model input parameters

Table 1 presents the input parameters used in the model based on the experimental condition and also the model assumptions. The outputs of the model are the concentration of ions in the membrane, fluxes, the membrane voltage drop, and the sodium transport number.

3 Results and discussion

Figure 3 shows the profiles of concentration change for sodium, hydroxide, and water in the membrane over a dimensionless length of the membrane at the steady-state.

The identical concentrations in the anolyte and catholyte bulk solution are shown as straight lines followed by the gradient in the boundary layer thickness. The concentration inside the membrane stands between the two vertical lines. Increasing the current density results in a lower concentration of ions in the membrane on the anode side and a higher concentration on the cathode side.

Figure 4 shows that the voltage drop and sodium transport numbers calculated for the model with constant porosity and active number of pores do not fit with the measured values in the experiment. The experiments were carried out on the mono layer Nafion N-1110 in an identical solution of 15 wt% sodium hydroxide at 40 °C [12]. The model shows a linear increase of the membrane voltage drop with current density and no dependence of sodium transport number on the current density. Since the model is unable to predict the membrane performance as a function of current density, the membrane swelling assumption as described in Sect. 2 is used to describe the membrane behavior at high current densities. As there are no measured data available for a change of membrane structure due to swelling, a range of pore diameters and number of active cylindrical pores are chosen based on the rough estimation of the found pore diameters in the literature [7, 8].

Figures 5a, b presents the sensitivity analysis of the model over a range of membrane pore diameters, and active numbers of cylindrical pores at 10 and 20 kA m⁻², respectively, for 2 × 10¹⁶ total number of the pores. The total number of pores is calculated from the properties presented in Table 1. It shows that for a certain total number of pores, there is a unique set of channel diameter and active number of pores that fit to the experimental values of the membrane voltage drop and sodium transport number.

Table 1 Input parameters of the model

Parameter	Value	Reference
Temperature (°C)	40	
Sodium diffusivity in free water (m ² s ⁻¹)	1.33 × 10 ⁻⁹	[45]
Hydroxide diffusivity in free water (m ² s ⁻¹)	5.27 × 10 ⁻⁹	[45]
Water diffusivity in membrane (m ² s ⁻¹)	2.8 × 10 ⁻¹⁰	[46]
Mass transfer coefficient in solution ^a (m s ⁻¹)	1 × 10 ⁻⁴	
Sodium hydroxide viscosity (kg m ⁻¹ s ⁻¹)	1.44 × 10 ⁻³	[17]
Dry membrane thickness (m)	2.54 × 10 ⁻⁴	[36]
Wet membrane thickness ^b (m)	2.7 × 10 ⁻⁴	
Dry membrane density (kg m ⁻³)	2 × 10 ³	[47]
EW (-)	1100	[36]
Membrane porosity (m ³ _{void} /m ³ _m)	0.27	[48, 49]
Sodium hydroxide concentration in both anolyte and catholyte (wt%)	15	
Membrane water content (wt% dry polymer)	Correlation	[17]
	1	[42]

^a Measured in a rotor–stator spinning disc reactor [50]

^b Measured with a digital caliper

Fig. 3 Concentration profiles of **a** sodium ions, **b** hydroxide ions, and **c** water inside the N-1110 membrane at the steady-state for current density range of 0–20 kA m^{-2} in 15 wt% sodium hydroxide solution as both analyte and catholyte

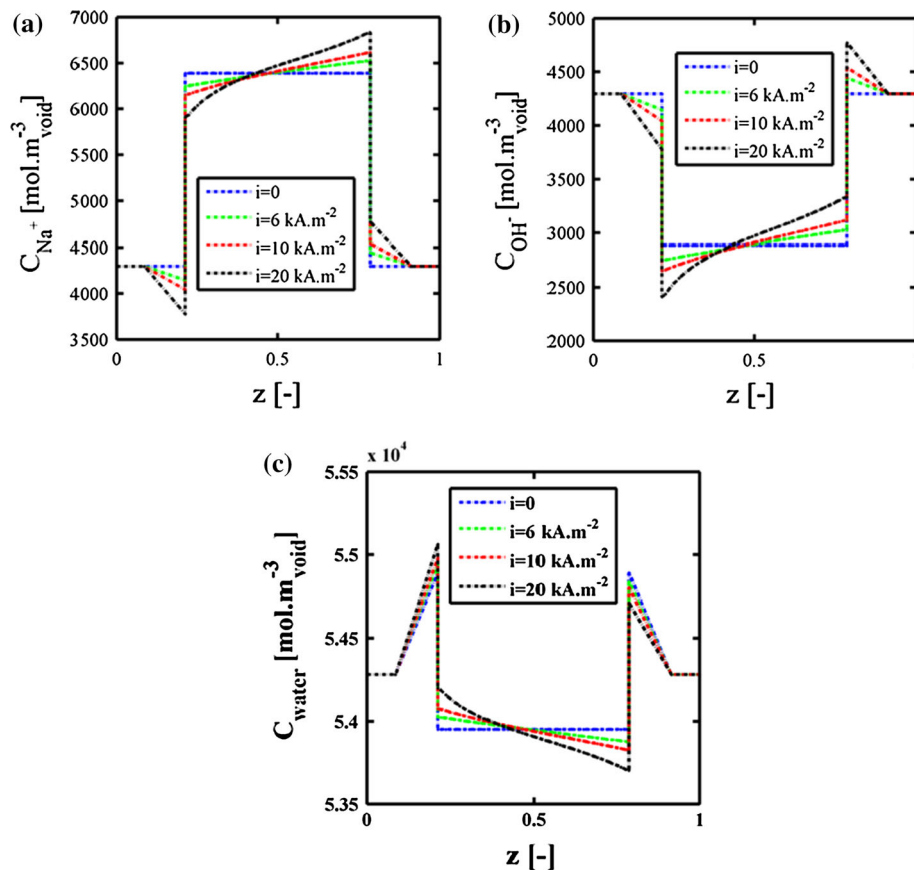
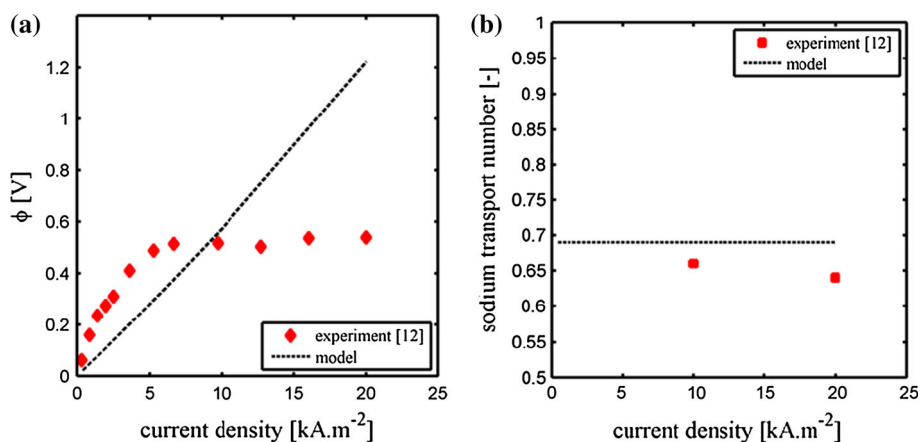


Fig. 4 Membrane **a** voltage drop and **b** sodium transport number at the steady-state and current density range of 0.3–20 kA m^{-2} measured experimentally [12] and calculated for the base model



The sensitivity analysis was performed at other current densities to fit the model to the experimentally measured values of the membrane voltage drop and sodium transport number. The fitted pore diameter and number of active pores used in the model that matched the experimental values of the voltage drop are presented in Fig. 6. The transport number is only fitted at the two available values of 10 and 20 kA m^{-2} . Figure 6a shows how the pore diameter increases with increasing current density. Figure 6b shows the opening of the dead-end pores and activation of more cluster channels in transporting the ions

though the membrane as a function of current density. This shows that increasing the current density results in swelling of the membrane due to an increase in channel diameter. Also, it predicts that with an increase in the current density, the number of active pores that participate in the ion transport increases, and possibly some of the dead-end pores open at high current densities. This way the model is able to give a better prediction of ion transport inside the membrane. At this stage, no better reasoning could be found to explain the observed trend of change in the membrane voltage drop and transport number with

Fig. 5 Sensitivity analysis of membrane voltage drop and sodium transport number over a range of pore diameters (*solid line* d_p , nm) and numbers of active pores (*dashed line* $N_{act} \times 10^{-15}$) for a given 2×10^{16} total number of pores. The experimental membrane voltage drop and sodium transport number (*dot*) at **a** 10 kA m^{-2} and **b** 20 kA m^{-2} [12]

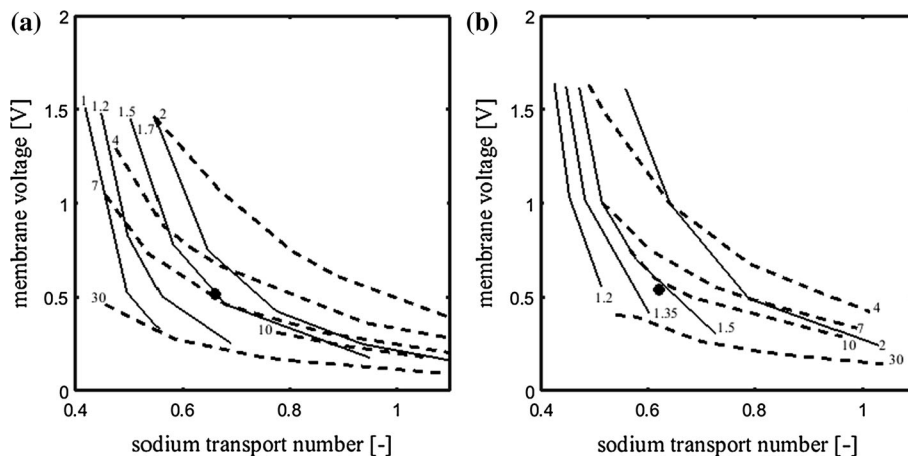
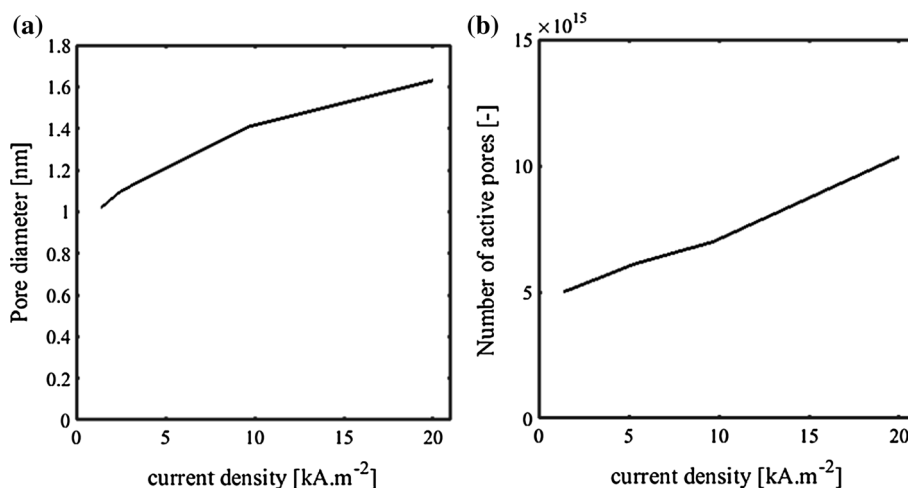


Fig. 6 The effect of current density on the membrane swelling and opening up of **a** the pore clusters and **b** the dead-end pores



increasing current density. The proposed values of the channel diameter for a swollen membrane by others [7, 8] are an average of 20 nm for solutions other than sodium hydroxide which could be the reason of the different obtained optimized channel diameters here. It is worth mentioning that using the optimized channel diameters and the number of active pores at different current densities did not change the concentration profiles of the ions and water in the membrane.

4 Conclusion

The transport of ions and water through a cation-exchange membrane has been mathematically modeled using the Nernst–Planck equation. For a single-layer Nafion N-1110 membrane, the model has been fitted to the measured values of the membrane voltage drop and sodium transport number at high current densities up to 20 kA m^{-2} using the membrane swelling assumption. Also, it is shown that the model is very sensitive to the pore diameter and the number

of active pores. This could be because these parameters are a function of current density. Currently, we cannot find another reason to explain the observed behavior. With increasing current density, more charged ions rush into the membrane. Therefore, the membrane conductivity increases with current density. The change in pore diameter and number of active pores cannot be measured under transport conditions. The qualitative swelling model can explain the behavior of the membrane pore clusters at high current density.

We conclude that at high current densities the diameter of the pore channels is likely to increase due to the membrane swelling. This results in a higher number of active pores participating in transport of the ions through the membrane. It is believed that the membrane structure, i.e., channel size and porosity, has a high impact on the performance of this membrane in sodium hydroxide solution. Furthermore, it shows that there is a unique set of pore diameters and number of active pores that satisfy the experimental sodium transport number at a certain membrane voltage drop. This suggests that having a more in-

depth knowledge of the membranes structure in a molecular level helps better understanding the ion transport in extreme operating conditions such as high current density.

Acknowledgments This project is funded by the Action Plan Process Intensification of the Dutch Ministry of Economic Affairs (Project PI-00-04).

Open Access This article is distributed under the terms of the Creative Commons Attribution 4.0 International License (<http://creativecommons.org/licenses/by/4.0/>), which permits unrestricted use, distribution, and reproduction in any medium, provided you give appropriate credit to the original author(s) and the source, provide a link to the Creative Commons license, and indicate if changes were made.

Appendix 1: Non-linear potential gradient

The electroneutrality condition (24) should hold in the membrane. Moreover, electroneutrality should be valid on either side of the membrane as well, Eq. (25). Furthermore, because the fixed group concentration is constant in the membrane, the summation of diffusional flux of positive charges equals the summation of diffusional flux of negative charges (26). This means that the total summation of diffusional fluxes is zero (27).

$$\sum_{i=1}^n z_i C_i + z_m C_m = 0, \quad (24)$$

$$\left(\sum_{i=1}^n z_i C_i \right)^L = \left(\sum_{i=1}^n z_i C_i \right)^R, \quad (25)$$

$$\left(\sum_{i=1}^n z_i D_i C_i \right)^L = \left(\sum_{i=1}^n z_i D_i C_i \right)^R, \quad (26)$$

$$\sum_{i=1}^n z_i D_i \nabla C_i = 0. \quad (27)$$

Also, the flux on right and left sides of the membrane should be equal at steady-state (28). Eq. (29) is derived by writing the flux equations for the left and right sides and using Eq. (7). The convective term is neglected in the flux equations.

$$J_i^L = J_i^R, \quad (28)$$

$$\begin{aligned} \frac{I}{F} &= - \left(\sum_{i=1}^n z_i D_i \nabla C_i + \sum_{i=1}^n z_i^2 D_i \nabla C_i \frac{F}{RT} \nabla \varphi \right)^L \\ &= - \left(\sum_{i=1}^n z_i D_i \nabla C_i + \sum_{i=1}^n z_i^2 D_i \nabla C_i \frac{F}{RT} \nabla \varphi \right)^R. \end{aligned} \quad (29)$$

By omitting the diffusional term [based in Eq. (26)], Eq. (30) is derived after a few rearrangements, and assuming that the potential gradient is constant, Eq. (30) contradicts from electroneutrality condition (25).

$$\left(\sum_{i=1}^n z_i^2 D_i C_i \right)^L = \left(\sum_{i=1}^n z_i^2 D_i C_i \right)^R. \quad (30)$$

Appendix 2: Transport equations

The material balance is needed (31) to describe the transport of ions due to diffusion, electro-migration, and convection inside the membrane. As explained, these three transport terms are described with the Nernst–Planck equation. Eq. (31) can be made dimensionless by substituting Eq. (32) in Eq. (31).

$$\frac{dC_i}{dt} = \nabla(J_i), \quad (31)$$

$$\frac{x}{\delta} = z, \quad (32)$$

$$\delta \frac{dC_i}{dt} = \frac{d}{d(z)} \left(\frac{1}{\delta} \left(-D_i \frac{dC_i}{dz} - z_i D_i C_i \frac{F}{RT} \frac{d\varphi}{dz} + v C_i \delta \right) \right), \quad (33)$$

$$v = \frac{d_h}{\delta} (z_m C_m F \nabla \varphi - \nabla P), \quad (34)$$

$$\frac{d\varphi}{dz} = \frac{\frac{I\delta}{F} + \sum_{i=1}^n z_i D_i \nabla C_i - v \sum_{i=1}^n z_i C_i}{-\frac{F}{RT} \sum_{i=1}^n z_i^2 D_i C_i}. \quad (35)$$

Appendix 3: Donnan equilibrium at the interface

Derivation of the solution interface concentration as a function of the membrane interface concentration

Recalling the Donnan equilibrium in which the osmotic contribution is neglected, Eq. (13), one can obtain (36) and (37) for the positive and negative species, respectively.

$$C_{i,\text{pos}}^{A,\text{int}} = C_{i,\text{pos}}^M \cdot \frac{1}{K}, \quad (36)$$

$$C_{i,\text{neg}}^{A,\text{int}} = C_{i,\text{neg}}^M \cdot K \quad (37)$$

By combining the electroneutrality in the solution with (36) and (37), (38) is obtained. After rearrangement of Eq. (38), an expression for Donnan constant K is presented in (39).

$$\sum_i^{N_{\text{ions}}} C_{i,\text{pos}}^M \cdot \frac{1}{K} = \sum_i^{N_{\text{ions}}} C_{i,\text{neg}}^M \cdot K, \quad (38)$$

$$K = \sqrt{\frac{\sum_i^{N_{\text{ions}}} C_{i,\text{pos}}^M}{\sum_i^{N_{\text{ions}}} C_{i,\text{neg}}^M}}. \quad (39)$$

Substitution of (39) in (36) and (37) results in (40) and (41), respectively. For a system of only sodium and hydroxide, (40) and (41) reduce to (42).

$$C_{i, \text{pos}}^{A, \text{int}} = C_{i, \text{pos}}^M \sqrt{\frac{\sum_i^{N_{\text{ions}}} C_{i, \text{neg}}^M}{\sum_i^{N_{\text{ions}}} C_{i, \text{pos}}^M}}, \tag{40}$$

$$C_{i, \text{neg}}^{A, \text{int}} = C_{i, \text{neg}}^M \sqrt{\frac{\sum_i^{N_{\text{ions}}} C_{i, \text{pos}}^M}{\sum_i^{N_{\text{ions}}} C_{i, \text{neg}}^M}}, \tag{41}$$

$$C_{\text{Na}^+}^{A, \text{int}} = \sqrt{C_{\text{Na}^+}^M \cdot C_{\text{OH}^-}^M}. \tag{42}$$

Derivation of the membrane interface molality as a function of the solution interface molality

From Eq. (13), (43) and (44) are obtained for the positive and negative species, respectively.

$$C_{i, \text{pos}}^M = C_{i, \text{pos}}^{A, \text{int}} \cdot K, \tag{43}$$

$$C_{i, \text{neg}}^M = C_{i, \text{neg}}^{A, \text{int}} \cdot \frac{1}{K}. \tag{44}$$

By combining the electroneutrality in the membrane with (43) and (44), (45) is derived. After rearrangement of (45), a quadratic expression for K is obtained, see (46). This quadratic expression can be solved resulting in (47).

$$\sum_i^{N_{\text{ion}}} C_{i, \text{pos}}^{A, \text{int}} \cdot K - C_m = \sum_i^{N_{\text{ion}}} C_{i, \text{neg}}^{A, \text{int}} \cdot \frac{1}{K}, \tag{45}$$

$$\sum_i^{N_{\text{ion}}} C_{i, \text{pos}}^{A, \text{int}} \cdot K^2 - C_m K - \sum_i^{N_{\text{ion}}} C_{i, \text{neg}}^{A, \text{int}} = 0, \tag{46}$$

$$K = \frac{C_m \pm \sqrt{C_m^2 + 4 \sum_i^{N_{\text{ion}}} C_{i, \text{pos}}^{A, \text{int}} \sum_i^{N_{\text{ion}}} C_{i, \text{neg}}^{A, \text{int}}}}{2 \sum_i^{N_{\text{ion}}} C_{i, \text{pos}}^{A, \text{int}}}. \tag{47}$$

Substitution of (47) in (43) and (44) results in (48) and (49), respectively. For a system of only sodium and hydroxide, (47) reduces to (50).

$$C_{i, \text{pos}}^M = C_{i, \text{pos}}^{A, \text{int}} \frac{C_m + \sqrt{C_m^2 + 4 \sum_i^{N_{\text{ion}}} C_{i, \text{pos}}^{A, \text{int}} \sum_i^{N_{\text{ion}}} C_{i, \text{neg}}^{A, \text{int}}}}{2 \sum_i^{N_{\text{ion}}} C_{i, \text{pos}}^{A, \text{int}}}, \tag{48}$$

$$C_{i, \text{neg}}^M = C_{i, \text{neg}}^{A, \text{int}} \frac{2 \sum_i^{N_{\text{ion}}} C_{i, \text{pos}}^{A, \text{int}}}{C_m + \sqrt{C_m^2 + 4 \sum_i^{N_{\text{ion}}} C_{i, \text{pos}}^{A, \text{int}} \sum_i^{N_{\text{ion}}} C_{i, \text{neg}}^{A, \text{int}}}}, \tag{49}$$

$$C_{\text{Na}}^M = \frac{C_m + \sqrt{C_m^2 + 4 (C_{\text{Na}^+}^{A, \text{int}})^2}}{2}. \tag{50}$$

Prove that (42) and (50) are equal

Substitution of the electroneutrality condition in the membrane in (50), (42) is obtained with (51) as an intermediate result.

$$C_{\text{Na}^+}^{A, \text{int}} = \sqrt{(C_{\text{Na}^+}^M)^2 - C_{\text{Na}^+}^M C_m}. \tag{51}$$

References

1. Rohman FS, Aziz N (2008) Mathematical model of ion transport in electrodialysis process. *Chem React Eng Catal* 3:3–8
2. Psaltis STP, Farrell TW (2011) Comparing charge transport predictions for a ternary electrolyte using the maxwell-stefan and nernst-planck equations. *J Electrochem Soc* 158:A33
3. Graham EE, Dranoff JS (1982) Application of the Stefan–Maxwell Equations to diffusion in ion exchangers. 1. Theory. *Am Chem Soc* 21:360–365
4. Fujimura M, Hashimoto T, Kawai H (1982) Small-angle X-ray scattering study of perfluorinated ionomer membranes. 2. Models for ionic scattering maximum. *Am Chem Soc* 15:136–144
5. Haubold H, Vad T, Jungbluth H, Hiller P (2001) Nano structure of NAFION: a SAXS study. *Electrochim Acta* 46:1559–1563
6. Mauritz KA, Moore RB (2004) State of understanding of Nafion. *Chem Rev* 104:4535–4585
7. Schmidt-Rohr K, Chen Q (2008) Parallel cylindrical water nanochannels in Nafion fuel-cell membranes. *Nat Mater* 7:75–83
8. Gebel G (2000) Structural evolution of water swollen perfluoro-sulfonated ionomers from dry membrane to solution. *Polymer (Guildf)* 41:5829–5838
9. Verbrugge MW, Hill RF (1990) Ion and solvent transport in ion-exchange membranes I. A macrohomogeneous mathematical model. *Electrochem Soc* 137:886–893
10. Fila V, Bouzek K (2003) A mathematical model of multiple ion transport across an ion-selective membrane under current load conditions. *J Appl Electrochem* 33:675–684
11. Fila V, Bouzek K (2008) The effect of convection in the external diffusion layer on the results of a mathematical model of multiple ion transport across an ion-selective membrane. *J Appl Electrochem* 38:1241–1252
12. Moshtarikah S, de Groot MT, Keurentjes JTF, et al. (2016) Cation-exchange membrane performance under high current density. (in prep)
13. Strathmann H (2004) Ion-exchange membrane separation processes, 1st edn. Elsevier, Amsterdam
14. Sata T (2004) Ion exchange membranes; preparation, characterization, modification and application. The Royal Society of Chemistry, Cambridge
15. Schlögl R (1966) Membrane permeation in systems far from equilibrium. *Berichte der Bunsengesellschaft für Phys Chemie* 70:400–414
16. Schlögl R (1964) Stofftransport durch membranen. Steinkopff, The University of California, Darmstadt
17. O'Brien TF, Bommaraju TV, Hine F (2005) Handbook of Chlor–Alkali technology, volume I: fundamentals. Springer, New York
18. Okada T, Xie G, Gorseth O, Kjelstrup S (1998) Ion and water transport characteristics of Nafion membranes as electrolytes. *Electrochim Actamica Acta* 43:3741–3747
19. Stewart RJ, Graydon WF (1955) Ion-exchange membranes. III. Water transfer. *J. Phys. Chem*, p 61

20. Bourdillon C, Demarty M, Selegny E (1974) Transport of water in cation exchange membranes II. Influence of polarization layers in natural convection. *J Chim Phys* 71:819–827
21. Lakshminarayanaiah N (1969) Electroosmosis in ion-exchange membranes. *J Electrochem Soc* 116:338
22. Krol JJ (1969) Monopolar and bipolar ion exchange membranes: mass transport limitations. University of Twente, Enschede
23. Khedr G, Schmitt A, Varoqui R (1978) Electrochemical membrane properties in relation to polarization at the interfaces during electro dialysis. *Colloid Interface Sci.* 66:516–530
24. Fang Y, Li Q, Green ME (1982) Noise spectra of sodium and hydrogen ion transport at a cation membrane-solution interface. *Colloid Interface Sci* 88:214–220
25. Cooke BA (1961) Concentration polarization in electro dialysis-I. The electrometric measurement of interfacial concentration. *Electrochim Acta* 3:307–317
26. Taky M, Pourcelly G, Gavach C (1992) Polarization phenomena at the interfaces between an electrolyte solution and an ion exchange membrane Part II. Ion transfer with an anion exchange membrane. *Electroanal Chem* 336:195–212
27. Yamabe T, Seno M (1967) The concentration polarization effect in ion exchange membrane electro dialysis. *Desalination* 2:148–153
28. Simons R (1979) The origin and elimination of water splitting in ion exchange membranes during water demineralisation by electro dialysis. *Desalination* 28:41–42
29. Rubinsten I, Shtilman L (1978) Voltage against current curves of cation exchange membranes. *Chem Soc Faraday Trans 2 Mol-Chem Phys* 75:231–246
30. Rosenberg NW, Tirrell CE (1957) limiting currents in membrane cells. *Ind Eng Chem* 49:780–784
31. Block M, Kitchener JA (1966) Polarization phenomena in commercial ion-exchange membranes. *Electrochem Soc* 113:947–953
32. Tanaka Y (2012) Mass transport in a boundary layer and in an ion exchange membrane: mechanism of concentration polarization and water dissociation. *Russ J Electrochem* 48:665–681
33. Ho PC, Palmer DA (1995) Electrical conductivity measurements of aqueous electrolyte solutions at high temperatures and high pressures. In: Proceedings of the 12th international conference on the properties of water and steam
34. Higa M, Tanioka A, Miyasaka K (1988) Simulation of the transport of ions against their concentration gradient across charged membranes. *J Memb Sci* 37:251–266
35. Meeuwse M (2011) Rotor-stator spinning disc reactor. Eindhoven University of Technology, Eindhoven
36. Majsztzik P, Bocarsly A, Benziger J (2008) Water permeation through Nafion membranes: the role of water activity. *Phys Chem* 112:16280–16289
37. Wesselingh JA, Vonk P, Kraaijeveld G (1995) Exploring the Maxwell–Stefan description of ion exchange. *Chem Eng* 57: 75–89
38. Marshal TJ (1957) Permeability and the size distribution of pores. *Nature* 180:664–665
39. Millington RJ (1959) Gas diffusion in porous media. *Science* 130:100–102
40. Weissberg HL (1963) Effective diffusion coefficient in porous media. *J Appl Phys* 34:2636
41. Neale GH, Nader WK (1973) Prediction of transport processes within porous media: diffusive flow processes within an homogeneous swarm of spherical particles. *AIChE J* 19:112–119
42. Yeo RS (1983) Ion clustering and proton transport in Nafion membranes and its applications as solid polymer electrolyte. *J Electrochem Soc* 130:533–538
43. Berezina NP, Kononenko NA, Dyomina OA, Gnsin NP (2008) Characterization of ion-exchange membrane materials: properties vs structure. *Adv Colloid Interface Sci* 139:3–28
44. Takahashi Y, Obanawa H, Noaki Y (2001) New electrolyser design for high current density. *Mod. Chlor-Alkali Technol.* 8:8
45. Samson E, Marchand J, Snyder KA (2003) Calculation of ionic diffusion coefficients on the basis of migration test results. *Mater Struct* 36:156–165
46. Suresh G, Scindia Y, Pandey A, Goswami A (2005) Self-diffusion coefficient of water in Nafion-117 membrane with different monovalent counterions: a radiotracer study. *J Memb Sci* 250: 39–45
47. DuPont Fuel Cells, Technical information. 0–3
48. Tiss F, Chouikh R, Guizani A (2013) A numerical investigation of the effects of membrane swelling in polymer electrolyte fuel cells. *Energy Convers Manag* 67:318–324
49. Chi PH, Chan SH, Weng FB et al (2010) On the effects of non-uniform property distribution due to compression in the gas diffusion layer of a PEMFC. *Int J Hydrogen Energy* 35:2936–2948
50. Granados Mendoza P (2016) Liquid solid mass transfer to a rotating mesh electrode. *Heat Mass Transf* (Submitt)